Advanced Turboprop Transport Aircraft Modeling for the Electrified Powertrain Flight Demonstration Project

Dahlia D. V. Pham, Jeffrey V. Bowles, Carl Recine, and Susie Go
NASA Ames Research Center, Moffett Field, CA, USA

The objective of this study is to establish models for state of the art, representative regional non-electrified turboprop configurations in the 19 to 50 passenger capability range and assess performance impacts from advanced aircraft technologies. Two of these models will serve as reference baseline configurations for comparison to electrified aircraft propulsion (EAP) demonstrator concepts for the Electrified Powertrain Flight Demonstration (EPFD) project. The other two non-electrified configurations will primarily assess the impacts of advanced technologies on fuel consumption and CO_2 emissions. This paper details an aircraft synthesis and performance analysis approach using the General Aviation Synthesis Program (GASP) which is used to establish baseline performance capabilities, calibrate airplane and engine models using published manufacturer data and conduct technology sensitivity studies. Advanced technologies are selected from the categories of propulsion, aerodynamics, and flight systems. A GASP-Monte Carlo simulation framework for uncertainty propagation is used to obtain performance distributions of the expected fuel burn, weight reduction and CO_2 emissions reductions from advanced aircraft technologies. Significant fuel burn savings from application of aerodynamics and propulsion technologies was observed.

Nomenclature

AEO	=	All Engines Operating
BSFC	=	brake-specific fuel consumption
c	=	chord length
CEI	=	Critical Engine Inoperative
ρ	=	air density
C_f	=	skin friction drag coefficient
C_d	=	2D drag coefficient
C_D	=	3D drag coefficient
C_L	=	3D lift coefficient
D	=	drag force
L	=	lift force
L/D	=	lift to drag ratio
n	=	load factor
OPR	=	overall pressure ratio
pax	=	passenger
shp	=	shaft horsepower
t	=	airfoil thickness
x_{tr}	=	transition location
Re	=	Reynolds number
S	=	Reference area
V_c	=	design cruise number

$(x, y, z)_{comp}$ = x, y, or z component location in the aft, right, up convention
TSFC = thrust-specific fuel consumption
T.O. = takeoff
W = weight

I. Introduction

Reducing fuel and overall energy consumption has long been the goal of the commercial aviation industry. In the United States Aviation Climate Action Plan [1], the Federal Aviation Administration (FAA) reported that more than 97% of U.S. aviation CO_2 emissions is derived from the combustion of jet fuel, where 80% of domestic aviation emissions come from enroute operations above 10,000 feet [1]. The report also detailed the government-wide approach to steer the aviation sector on a path toward achieving net zero emissions by 2050. Additionally, the National Aeronautics and Space Administration (NASA) Aeronautics Research Mission Directorate (ARMD) through the Environmentally Responsible Aviation (ERA) and Electrified Powertrain Flight Demonstration (EPFD) programs aims to facilitate the development of advanced aircraft technologies that reduce emissions across various vehicle classes and power levels, including 19 to 50 passenger turboprop transport aircraft.

The NASA ARMD Strategic Implementation Plan has set reduced fuel burn and consequently emissions as a primary goal for future commercial aircraft development [2]. Such projects have included the ERA project followed by the current EPFD project, which both aim to enable vehicle concepts and advanced technologies that will reduce the impact of aviation on the environment [3]. Regarding advanced technologies, the ERA project has set an aircraft fuel reduction goal of 50-60% [4]. Since fuel burn reduction leads to reduced CO_2 emissions and better operating economy, both ERA and EPFD have identified the regional aircraft market, which consists of short-haul cargo and commuter operations, as a high-impact area for integrating advanced technologies into the commercial air travel space [4]. With revolutionary energy efficiency and environmental compatibility as the forefront vision for fixed wing transport aircraft under NASA ARMD, previous work done by the Advanced Air Transport Technology (AATT) project has scoped advanced technologies to enable that vision [5]. In 2019, researchers at Georgia Institute of Technology published a technical report under the AATT project enclosing a comprehensive portfolio of advanced technologies that would be of interest to sustainable flight programs such as ERA and EPFD [6]. This portfolio serves as reference for the advanced technologies selected in this paper.

The impact of advanced aircraft technologies on flight performance has previously been modeled using statistical generalizations [6, 7, 8]. However, uncertainties are prevalent at every phase of aircraft systems analysis due to the variability of performance inherent with certain advanced technologies where omission of uncertainty may lead to under- or over-design [9]. Though many systems analysts are aware of the prominence of uncertainty in their assessments, very few studies have incorporated methods to address and characterize this uncertainty [10]. Thus, for programs such as ERA, EPFD, and AATT, coupling of modeling & simulation (M&S) environments with uncertainty propagation methods is of interest for more robust systems analysis. Specific implementation of Monte Carlo methods in M&S environments have been found to enable successful propagation of small uncertainties throughout performance assessments [8, 9, 10].

The objective of this study is to establish baseline, parametric models of identified state-of-the-art turboprop aircraft of interest to the EPFD program within an M&S environment for systems analysis. Using a portfolio of technologies selected from the AATT project, the baseline models will be infused with advanced aircraft technologies and assessed using the NASA/Georgia Institute of Technology-developed General Aviation Synthesis Program (GASP) coupled with Monte Carlo simulation to allow for technology sensitivity studies with uncertainty propagation. Performance distributions capturing the impact of advanced technologies on weight, fuel burn, and CO_2 emissions will be presented. Overall, this paper will detail the System Analysis team's independent approach to vehicle synthesis, calibration, impact assessment, Monte-Carlo parametric sensitivity studies, and modeling efforts to complement the EPFD and demonstrate our capabilities in assessing future EAP technologies and vision systems. Additionally, the results from this study will also determine the benefits from applying advanced technologies in terms of fuel consumption, CO_2 emissions and how it facilitates the 60-80% reduction goal in aircraft fuel/energy consumption beyond 2035stated in Ref. [2].

II. Tool Description

A. General Aviation Synthesis Program (GASP)

For this study, sizing and mission analysis of the aircraft is performed using the NASA-developed General Aviation Synthesis Program (GASP), a parametric modeling and mission analysis tool that emphasizes fixed-wing airplanes with turboprop/turbofan propulsion systems initially developed at NASA Ames Research Center and later enhanced at the Georgia Institute of Technology in the 1990s and has been enhanced over the years [11]. It is a useful M&S tool in the conceptual phase of the aircraft design process, using engineering-level analysis methods to perform configuration sizing and estimate flight performance characteristics.

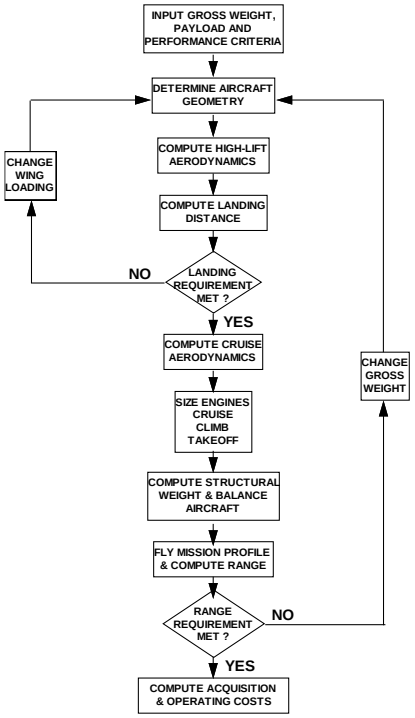

Figure 1. GASP Methodology and Modules

GASP is comprised of integrated technology modules that account for effects of design variables in the airplane design procedure which allows for configuration comparison, assessment of airplane performance and economics, and assessing the impact of advanced technologies on aircraft performance and operational performance. These six "technology" sub-modules perform the various independent functions required in the design of fixed-wing aircraft. The six modules include geometry, aerodynamics, propulsion, weight and balance, mission performance, and economics. These six technology modules are integrated into a single system by a control module shown in Figure 1. Other comparable programs are NASA Langley Research Center's Flight Optimization System Software (FLOPS), Stanford University's Program for Aircraft Synthesis Studies (PASS), and Georgia Institute of Technology's Electrified Propulsion Architecture Sizing and Synthesis (E-PASS) which all leverage semi-empirical models to capture aircraft performance sensitivities to input variables [7, 12]. As of 2022, both turboprop and turbofan versions of the GASP software have been updated to support analysis of EAP-enabled aircraft concepts to facilitate EPFD goals.

Parametric inputs such as public domain aircraft weight and geometry data, the mission profile, engine model, and technology sensitivity inputs are used to initialize GASP based on which vehicle is being synthesized and which technologies are being infused. Then, to size a vehicle, an input desired range and payload is applied, and GASP will iterate on the gross takeoff weight required to match the desired range, including the reserve mission fuel, using the Newton-Raphson iterative method where the error derivatives are computed using finite difference methods. When the fuel required and fuel available are equivalent, the program will produce outputs of the aircraft trajectory, weight, aerodynamics, and propulsion breakdowns for each specified flight mission phase. This integrated approach ensures that the results from each module contain the effect of design interactions among all the modules, and advanced aircraft technologies can be infused parametrically within their respective module.

B. Uncertainty Propagation with Monte Carlo Simulation

When studying the impact of advanced aircraft technologies on sizing and conceptual design of airplane concepts, it is important to consider that any performance assessment at this stage inherently propagates uncertainties [10]. Previously, systems analysts have often modeled the effects of advanced technologies using fixed input parameters obtained through historical data collection or, subject matter expert (SME) derived point estimates. Then, using M&S tools such as GASP, PASS, and FLOPS, deterministic analyses are run to produce single output aircraft performance estimates. However, deterministic analyses do not consider the stochastic nature of the uncertainties present in aircraft operating conditions, manufacturing processes, and even data collection methodology that may cause variation in performance [9]. Therefore, a Monte Carlo simulation framework is used for uncertainty propagation in tandem with GASP to quantify the impact of these uncertainties on estimated aircraft performance.

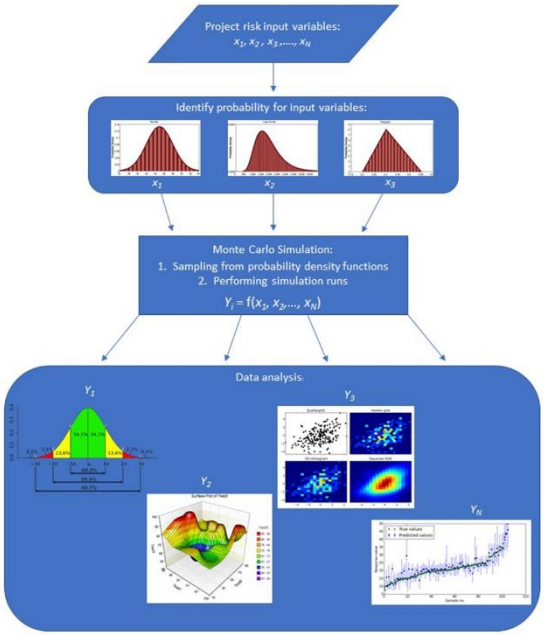

Figure 2. Monte Carlo Simulation Analysis © NASA 2017 [13]

A Monte Carlo (MC) simulation framework is a probabilistic analysis technique that uses random sampling to generate many possible outcomes and then calculates the probability distribution of those outcomes to determine likelihood of obtaining different results [9, 13]. Within this study, Python scripts are used to create an interface between the MC simulation framework and GASP to automate the generation of input parameter probability distributions, execute GASP to perform aircraft sizing and performance calculations, and obtain performance distributions that can provide insight into the expected behavior of the vehicle system and its associated uncertainties. In this framework, the input parameters for a system are represented as probability distributions, rather than fixed values. The simulation then samples from these distributions to create user-specified number of discrete events, each with different parameter values, and computes the outcome for each scenario. By aggregating the outcomes across all scenarios, MC simulations allow for a simple way of implementing uncertainty propagation to advanced aircraft technology performance assessment in the conceptual design phase.

III. Vehicle Synthesis

A. Geometry and Weight

Four candidate turboprop configurations have been identified for study: the Beechcraft 1900D, the Avions de Transport Régional/Aerei da Transporto Regional ATR-42-600, the de Havilland DHC-7-100, and Saab 340B. The Beechcraft 1900D and ATR 42-600 were selected as technology reference aircraft (TRA) in Ref. [7] while the DHC-7-100 and Saab 340B have been identified as candidate EAP flight demonstrators for the EPFD project [14, 15].

Table 1. Baseline Reference Aircraft Configurations

Item	Beechcraft 1900D	ATR 42-600	DHC-7-100	Saab 340B
References	[7, 16, 17]	[7, 16, 18]	[16, 19]	[16, 20]
Design Capacity (pax)	19	48	50	34
Number of Engines	2	2	4	2
Engine	PT6A-67D	P&W-127M	PT6A-50	GE CT7-9B

The turboprop aircraft selected were all representative commuter Part 23 and 25 aircraft of varying design capacities from 19 pax to 50 pax, where key design specifications are shown in Table 1. The Beechcraft 1900D (B1900D) is the latest variant of Beechcraft's B1900 family and currently identified as a highly utilized 19 pax regional airliner. The B1900D is equipped with two Pratt & Whitney Canada PT6A-67D turboprop engines at 1,279 shp. The ATR 42-600 is a twin-turboprop regional airliner designed and manufactured by the European aircraft manufacturer ATR with a design capacity of 48 pax and is powered by two Pratt & Whitney Canada PW127M engines each with a maximum takeoff power rating of 2,160 shp [7, 18]. Both aircraft were selected as TRA models for Ref. [7]. Then, in April 2022, the two baseline flight demonstrator aircraft for EPFD were the DHC-7-100, a four-engine turboprop manufactured by de Havilland Canada known for its short takeoff and landing (STOL) capabilities with four Pratt & Whitney Canada PT6A-50 engines with a maximum takeoff power rating of 1,120 shp, and the Saab 340B, a twin-engine turboprop regional airliner powered by two General Electric GE CT7-9B turboprop engines producing 1,748 shp each [14, 15].

The gross geometric parameters and dimensions for each configuration were obtained from open literature. [10]. Using key dimensions from the to scale three-view drawings as a benchmark for the gross geometric parameters, estimated weight breakdowns for obtained for all four turboprop configurations. The weights of the subsystem components (e.g., wing, fuselage, etc.) were computed using the weight estimating relationships within GASP, which are functions of geometric parameters and flight loading conditions.

Table 2. Aircraft Estimated Weight (in lbf) Statement for all Baseline Turboprops

Subsystem	Beechcraft 1900D	ATR 42-600	DHC-7-100	Saab 340B
Structures	6,125	12,828	15,291	9,313
Wing	1,479	3,445	3,995	2,631
Empennage	270	713	810	488
Fuselage	2,812	6,112	6,117	3,871
Landing Gear	899	1,640	1,980	1,160
Engine Section	665	916	2,389	1,163
Propulsion	1,868	4,677	4,409	2,919
Primary Engines	1,037	2,198	2,486	1,779
Engine Installation	207	679	619	443
Fuel System	223	414	412	238
Propulsor	401	858	892	459
Flight Controls	302	807	764	508
Fixed Equipment	2,222	5,932	7,224	4,168
Empty Weight	10,402	24,243	27,688	16,909
Fixed Useful Load	465	1,248	1,301	1,037
Operating Empty Weight	10,873	25,491	28,989	17,946
Payload	3,800	10,053	9,500	6,460
Fuel	2,562	5,461	5,511	4,594
Gross Takeoff Weight	17,120	41,005	44,000	29,000

Table 2 displays the subsystem weight breakdown from GASP. For each vehicle, the conventional baseline model in GASP was calibrated against existing aircraft data based on publicly available manufacturer data that was obtained from conducting an open literature search on each vehicle.

Table 3. Baseline Aircraft Calibration and Validation Results from GASP

Parameter	Beechcraft 1900D	ATR 42-600	DHC-7-100	Saab 340B
Gross Takeoff Weight, lbf	17,229	41,005	44,000	29,000
Operating Empty Weight, lbf	10,873	25,491	29,236	17,946
Engine Rated Power, shp	1,279	2,160	1,120	1,748
Wing Area, ft^2	310	586	860	450
Wingspan, ft	58	81	93.25	70.33
Block Fuel (300 nm) lbf	1,726	1,733	2,760	1,265

The GASP models were calibrated to match the key design parameters of gross takeoff weight, operating empty weight, block fuel for specified design mission range, and engine-rated power stated in publicly available data. The top-level parameters are reported in Table 3.

B. Aerodynamics

Once the calculations carried out to specify the vehicle geometry and weights with sufficient detail, the aerodynamic characteristics can be obtained. Estimates of the vehicle aerodynamics are computed such as equivalent flat plate and wetted areas of aircraft components, drag build-ups from the component level (profile drag, lift-induced drag, and compressibility drag), and optimal flap settings. Within GASP, the equivalent flat plate area and skin friction drag from each aircraft component is computed. The total skin friction coefficient is then calculated as a semi-empirical function of the Mach and Reynolds number:

$$C_{f,total} = \frac{0.455}{\frac{1+0.144M_0^2}{\log(Re_L)^{2.58}}} \tag{1}$$

Where the flat plate area calculation has been since modified from Ref. [11] to now account for 'aerodynamic technology factors', which are reductions in skin friction and/or excrescence drag from the infusion of advanced aircraft technologies.

$$FE_i = f_{CALIB,i} * f_{TECH,i} * CK_i * C_{f,i} * S_{wet,i} \tag{2}$$

where:

FE_i = flat plate area for the i^{th} component to match published performance (ft^2)
f_{CALIBi} = calibration factor for i^{th} component to match published performance
f_{TECHi} = Technology adjustment factors for i^{th} component to reflect advanced aero technology
Ck_i = Form drag factor for i^{th} component = f(Geometry Only: $SWET_i$/SREF, t/c or fineness ratio, Sweep, Mach,…)

Within the aerodynamics subroutine, the low speed drag polars can be obtained from lift and drag calculations at cruise for all four baseline turboprop aircraft.

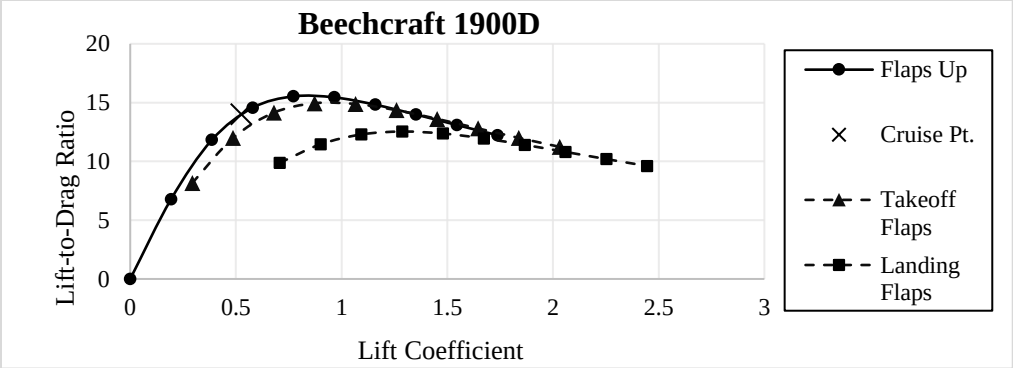

a) Beechcraft 1900D

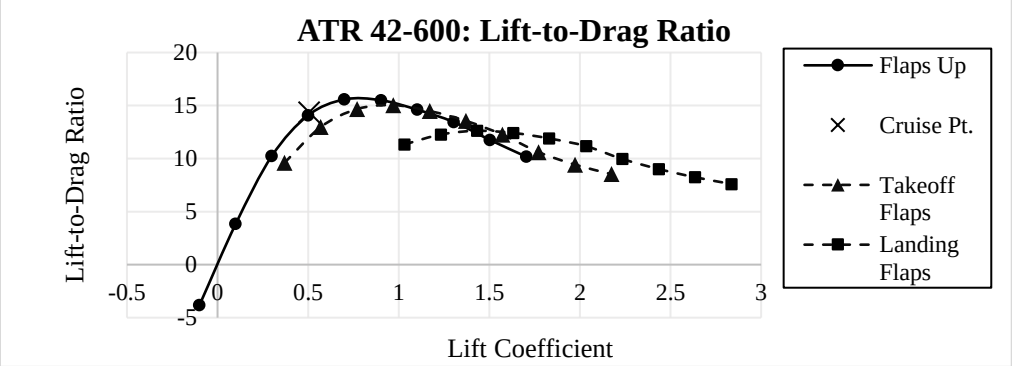

b) ATR 42-600

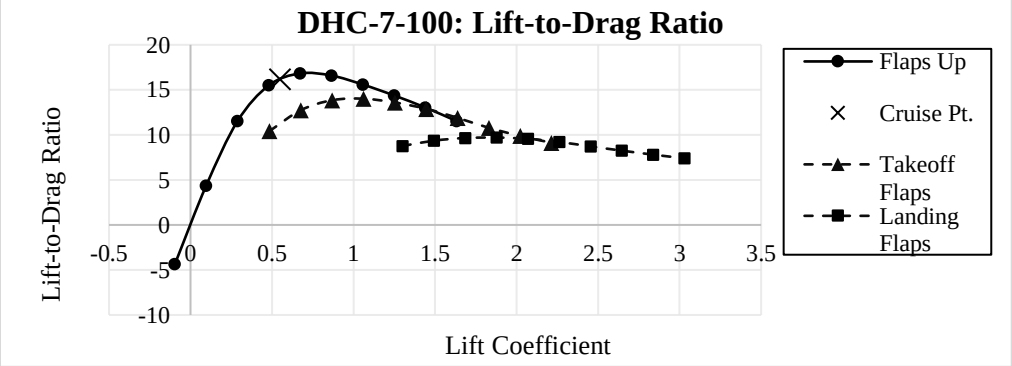

c) DHC-7-100

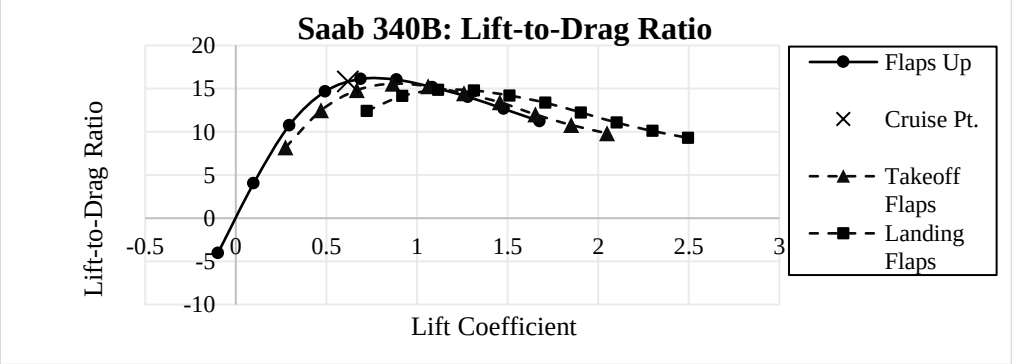

d) Saab 340B

Figure 3. Estimated Low-Speed Aerodynamics for the Baseline Turboprop Configurations

Figure 3 presents the lift-to-drag ratio as a function of the lift coefficient and flap configurations for the four baseline vehicles. The cruise points show the peak, untrimmed lift-to-drag ratios for the clean configuration of each vehicle. These models are functions of the geometric parameters and flight loading conditions.

C. Propulsion

The propulsion systems in the baseline GASP vehicle models are modeled using output engine models generated from the program Numerical Propulsion System Simulation (NPSS) developed by NASA Glenn Research Center that allows for the analysis and design of propulsion systems, such as the turboprop engines featured in this study. Engine performance parameters such as horsepower, fuel flow, and tail pipe thrust as a function of flight condition and power settings are provided in each engine model [8, 21].

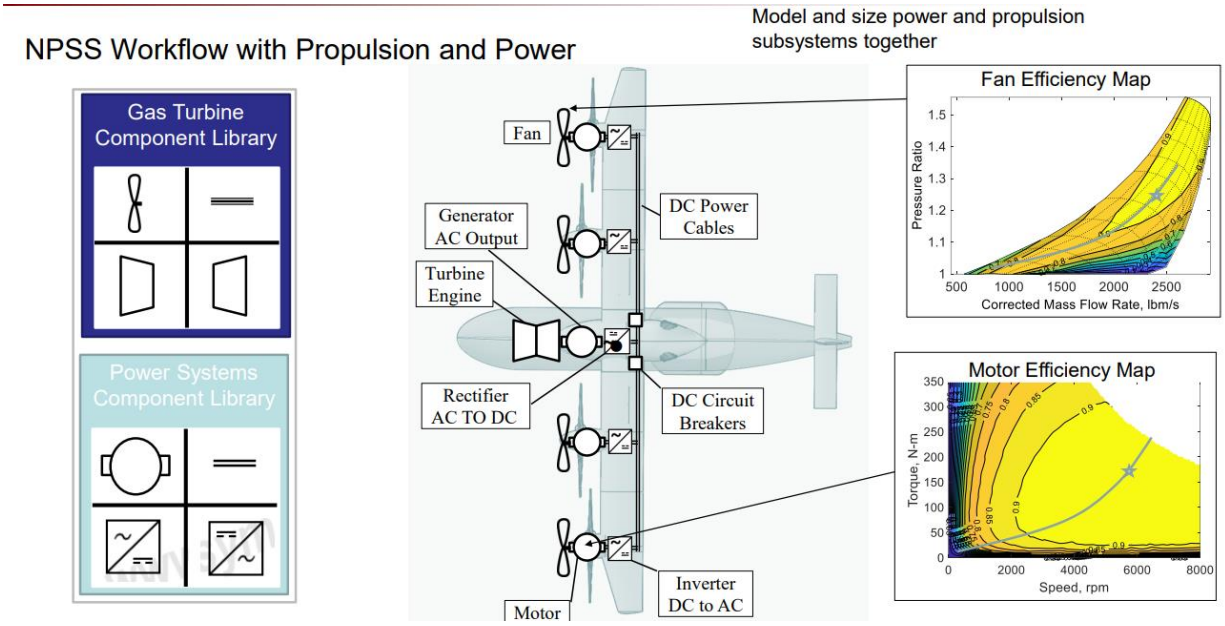

Figure 4. Typical Numerical Propulsion System Simulation (NPSS) Workflow [21]

Figure 4 depicts an example of the NPSS interface and its capabilities for modeling EAP-enabled aircraft concepts. The engine models were informed by type certificate data sheets (TCDS) publicly available online from the FAA and European Union Aviation Safety Agency (EASA), where non-proprietary engine models were synthesized that differed from publicly available data by ±3-4% to ensure omission of any proprietary information from EPFD project industry partners [8]. Then, within GASP, propeller calculations are done using Hamilton Standard propeller models [8, 11, 22]. Apart from published TCDS specifications, engine weights and dimensions were obtained from Ref. [23]. Lastly, engine installation effects are modelled using adjustment factors for the engine fuel flow.

C. Mission and Performance

With the weights model calibrated against published data and the aerodynamic and propulsion system modelled, the mission performance is computed by flying the vehicle along representative flight profiles. The mission profile shown is not to scale, where optimal speeds and altitude vary across the turboprop configurations.

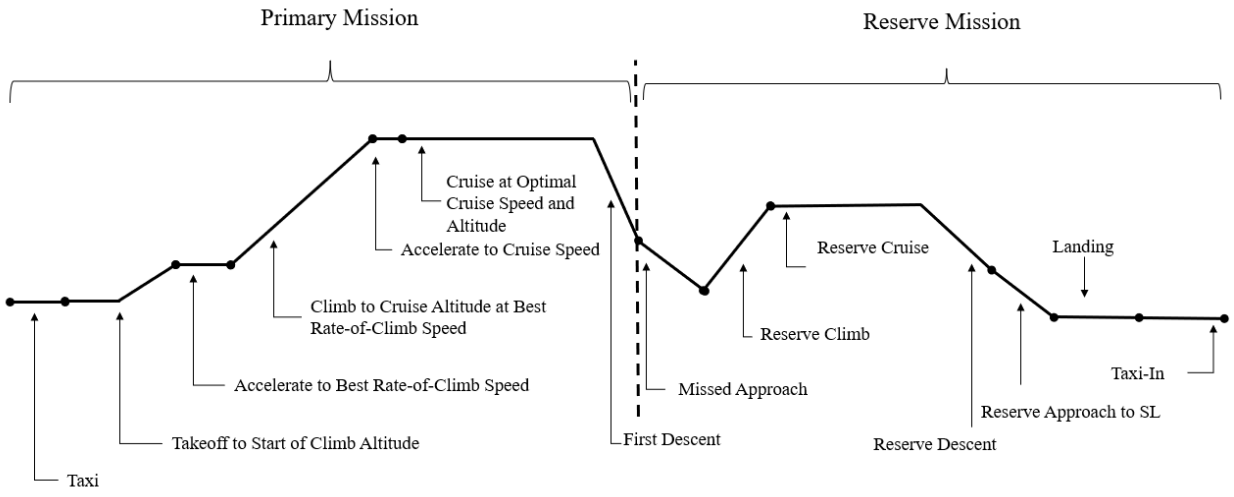

Figure 5. Generalized Reference Mission Profile

The reference mission flight profile used is shown in Figure 5. Using these missions, GASP is then able to compute the aircraft performance. Within GASP, the takeoff performance is calculated including gear and flap retraction. Then, a level flight segment accelerates the aircraft to the best rate-of-climb speed before climbing to the desired cruise speed at optimal altitude. Descent is flown at flight idle power setting at the optimal cruise Mach number, constrained if applicable by the fuselage pitch angle and maximum rate of sink. Then, the reserve mission is depicted, where an additional 3% mission fuel reserve allowance is prescribed. The vehicle then makes a missed approach, simulated by a two-minute time allocation at maximum takeoff power, and climbs out to the reserve mission altitude, where it cruises at a nominal Mach number for 100 nm to the alternate airport. For all vehicles, a four-minute time allowance for approach and landing is added along with an additional 45-minute hold flown at the best endurance speed. The performance characteristics for the aircraft are recorded at each phase of the mission.

Table 4. Baseline Vehicle Performance Parameters from GASP

Performance Parameter	**Beechcraft 1900D**	**ATR 42-600**	**DHC-7-100**	**Saab 340B**
AEO T.O. distance, ft	2250	3163	2109	3098
CEI T.O. distance, ft	2372	3630	2207	3209
Accelerate-Stop distance, ft	2700	3634	2643	2987
2nd Segment CEI Rate -of-climb, fpm	791	394	1012	335
Time to Climb to Cruise Altitude, min	15.41	20	18.84	12.88
Cruise Speed / Altitude, ktas/ft	250 / 25,000	200 / 25,000	220.5 / 21,000	252. / 19,000
Cruise Lift-to-Drag Ratio	15.07	14.37	15.69	14.49
Equivalent Flat Plate Area, ft^2	8.3592	15.12	21.02	12.18
Breguet Range Factor, nm	7378	9221	8378	8928
Specific range, nm/lb	0.4392	0.2294	0.1936	0.3132
BSFC, lb/hr/hp	0.6051	0.4669	0.5733	0.4853
TSFC, lb/hr/lbf	0.5105	0.4656	0.4135	0.4064

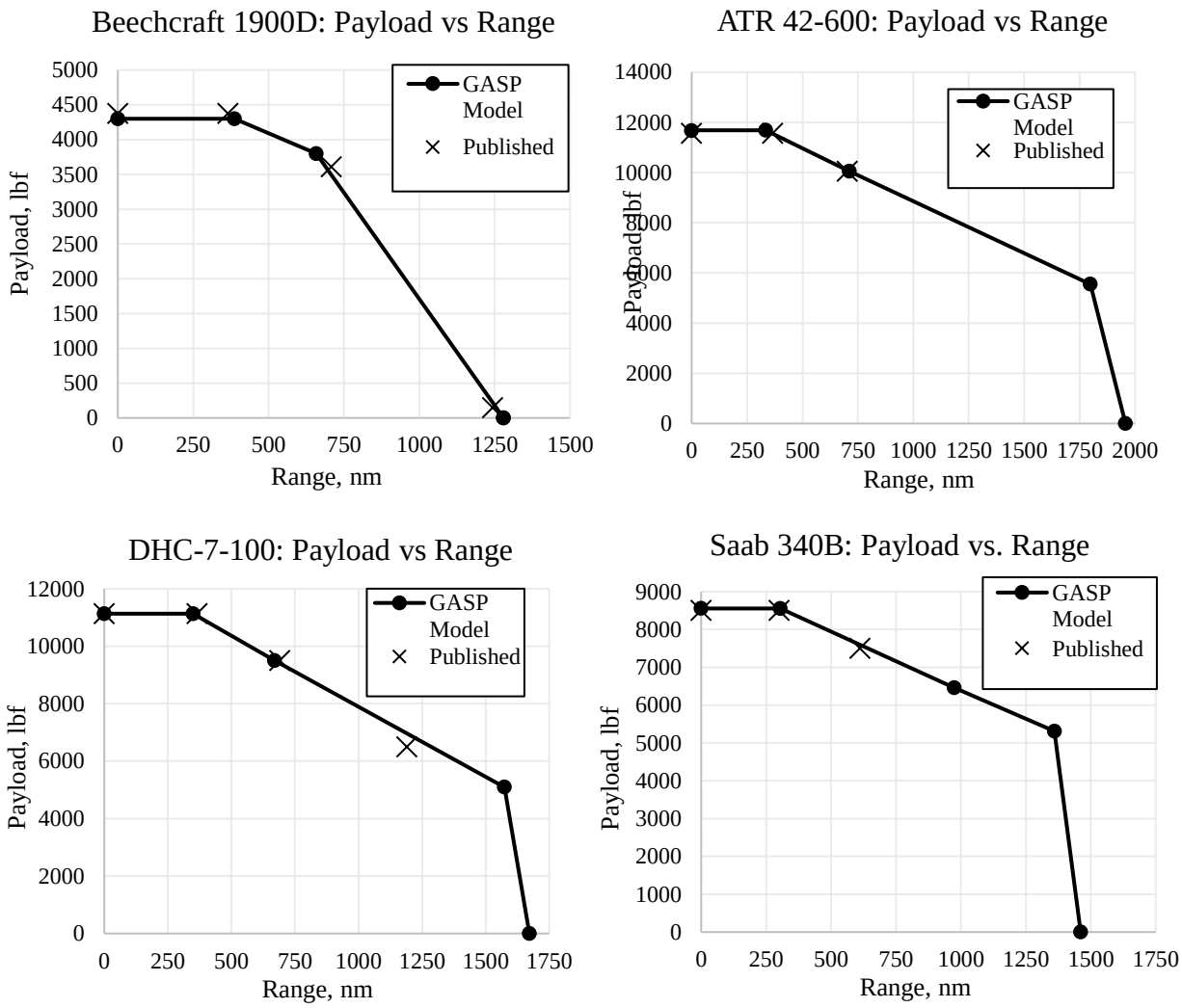

Figure 6. Payload vs. Range Calibration in GASP

Table 4 shows the baseline performance specification for each turboprop configuration, which will be used as benchmark values for the advanced turboprop configurations. Then, the fallout performance for various payload missions is then computed and the results shown in Figure 6. For the DHC-7, the range at maximum payload (11,100 lbf) is approximately 350 nm. The design payload of 9,500 lbf is estimated to be 680 nm. This compares favorably to the published value of 690 nm for the DHC-7 at the same payload weight [13]. And lastly, a payload of 6,500 lbf for the DHC-7 for an estimated range of 1,210 nm compares well with the published value of 1,190 nm [13]. The accuracy of the predicted ranges for the designated payload values is acceptable to establish a representative baseline configuration for the application of advanced technology and later serve as a reference for the application of electric aircraft propulsion (EAP) technology.

D. Advanced Technologies Selection

Prospective advanced technologies investigated were sorted by sub-group: propulsion, structures, aerodynamics, and flight systems. Table IV of Ref. [7] identifies several candidate advanced technologies for application to the 19 pax and 50 pax configurations along with the portfolio of technologies in Ref. [6]. Additionally, an independent literature review of current, in-development technologies for commercial transport aircraft was conducted, where a representative technology was selected for each category based off advanced aircraft technology reports from both

International Civil Aviation Organization (ICAO) and International Air Transport Association (IATA) [24, 25]. The technologies are then modeled onto the baseline aircraft where performance impacts are then assessed in GASP using the same mission profile where Monte Carlo parametric sensitivity studies are conducted to capture the distribution of expected performance.

Table 5. Advanced Technology Portfolio

Technology	Type	Description	Impact Area(s)
Damage-Arresting Composites (DAC)	Structures	Type of stitched structure composite technology developed with damage arrestment capabilities that prevent critical damage due to damage propagation, reduce airframe weight, and promises easier manufacturing processes by eliminating autoclave and tooling requirements [26].	Weight Reduction
Active Load Alleviation	Flight Systems	Active maneuver load and gust load alleviation systems allow for coordinated control deflections in response to maneuver and gust loads that aid with concentrating the lift inboard and reducing the wing bending moment, which reduces the wing weight [12].	Weight Reduction Load Alleviation
Riblets	Aerodynamics	V-Shaped grooves aligned with the direction of the flow that reduce the skin friction drag of turbulent boundary layers [27].	Drag Reduction
Natural Laminar Flow	Aerodynamics	Facilitates extended runs of laminar flow over an aircraft surface by passively stabilizing the boundary layer to produce significant drag reductions [7, 12].	Drag Reduction
Excrescence Reduction	Aerodynamics	Decreases parasite drag by imposing stricter tolerances in design and manufacturing [6].	Drag Reduction
Advanced Turboprop Engine Cycle & Materials	Propulsion	Expected evolutionary improvements in engine components and engine cycle design allowing for improved OPR, turbine temperatures and component efficiencies [7].	Propulsive Efficiency

Following the guidelines for advanced technologies presented in Ref. [9], the introduction of advanced composite structures offers the potential for significant empty weight reduction and the associated reduction in fuel consumption. The impact on fuselage and wing weight for composites relative to all metal construction will be assessed based on the recommendation of Ref. [13]. For engine performance, improvements in aerodynamic efficiencies, cycle design characteristics (OPR and turbine inlet temperatures and materials will result in improved engine performance and weight). For the 2030/35 time frame, a 15% improvement engine BSFC and 4% reduction in specific engine weight is assumed [14]. Candidate aerodynamic technologies are focused on the reduction of skin friction drag on various vehicle components. These include natural laminar flow control, riblet designs and various excrescence drag reduction approaches. Then, active load alleviation systems which combine both aerodynamic and structural benefits are studied to observe the sensitivities of simultaneous maneuver and gust load mitigation on weight and fuel burn reduction.

IV. Methodology

A. Advanced Technologies Modeling

In the previous sections, the baseline airframe configurations and engine models were calibrated and validated against publicly available data. With the baseline aircraft models established and technology portfolio synthesized, a robust methodology for modeling advanced aircraft technologies in GASP was formulated. Improving upon fixed-point estimates, the process for modeling advanced technologies involved historical data collection, literature review, formulation of semi-empirical models where applicable, and coupled iterative Monte-Carlo and GASP simulation to obtain performance distributions with uncertainty. For this study, advanced aircraft technologies are only applied to the wing-body structure, specifically the wing and the fuselage though extending the application methodology to the horizontal/vertical tails would be identical to that of the wing.

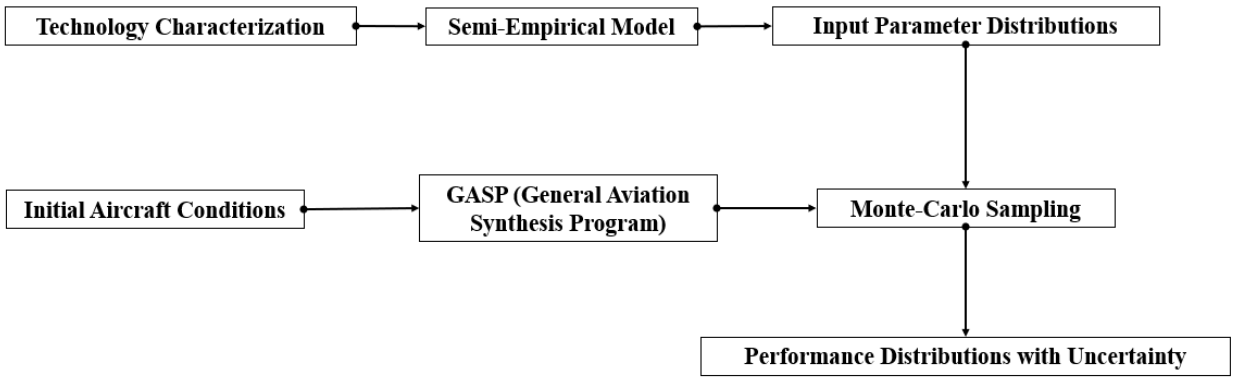

Figure 7. Advanced Aircraft Technology Modeling and Analysis

Within GASP, the impact of advanced technologies is quantified through technology characterization and semi-empirical modeling which informs the input parameter distributions. In Table 5, technologies are categorized by domain (e.g., aerodynamics, structures, propulsion) and impact area (e.g., weight reduction, drag reduction.) Before modeling the technologies in GASP, the quantified impact of the technology must be adequately characterized based on published performance estimates. The overall methodology for modeling advanced technologies is summarized in Figure 7.

Table 6. Advanced Aircraft Technology Characterization

Technology	Type	Technology Characterization
Damage-Arresting Stitched Composites (DAC)	Structures	Reduction in airplane component weights by at least 10 percent [28].
Active Load Alleviation	Flight Systems	Reduction in wing bending weight by 1.7% and load factor reduction from 2.5g to 1.8g [12, 30].
Riblets	Aerodynamics	Reduction in skin friction drag between 5-8% for airfoil sections and 1-6% on the fuselage [27]. In AATT, 2-8% skin friction drag on aircraft components is estimated [6].
Natural Laminar Flow	Aerodynamics	50% chord laminar flow on upper surface where applied [12] or, up to 80% chord laminar flow for multi-element wings and/or vortex generators [31, 32]
Excrescence Reduction	Aerodynamics	Reduction of 15-24% in profile drag equating to 8-12% reduction in cruise drag assuming full excrescence reduction [6] or, 7% of total drag reduction assuming full excrescence drag reduction [33].
Advanced Turboprop Engine Cycle & Materials	Propulsion	Approximately 10-15% improvement in engine BSFC due to improved OPR and T4 values and 4% reduction in specific engine weight from historical data-based projections [8, 34].

While analyses can be conducted after the technology characterization phase, semi-empirical modeling can further inform how advanced aircraft technologies are modeled in GASP. Semi-empirical models estimate aerodynamic characteristics of an aircraft based on coupling experimental data (e.g., from wind tunnel tests or flight tests) to physics-based equations (e.g., energy and momentum conservation.) Using semi-empirical models, advanced aircraft technologies can be modelled similarly to how aerodynamic characteristics of an aircraft are modeled in GASP—using applied aerodynamics theories and engineering-level analysis methods where applicable. Preliminary aircraft design sizing and optimization is based on well-established semi-empirical equations such as methods by Torenbeek and Hoerner which allow for efficient analyses on aircraft performance estimations, where GASP uses sizing equations from Torenbeek's methods in geometry, weight and performance estimations [11, 35].

For instance, semi-empirical models can allow the systems analyst to project two-dimensional aerodynamics effects onto three-dimensional components such as the wing and fuselage to predict the sensitivity a technology has on certain high-level aircraft design parameters such as the gross takeoff weight, operating empty weight, and fuel weight. For example, the impact of riblets can be modeled semi-empirically to obtain a distribution of expected skin friction drag reduction. Using empirical and analytical results from Ref. [27] to derive an equation similar to the semi-empirical methods discussed in Ref. [35], a semi-empirical model for riblets is determined as a function of wetted area coverage, the skin friction drag reduction cited in Table 6, and the ratio of skin friction to profile drag.

$$\Delta C_{D_{profile,riblet}} = \Delta C_f \frac{S_{wet,riblet}}{S_{wet,turb}} \frac{C_{D_{friction}}}{C_{D_{profile}}} \quad (3)$$

where:

$\Delta C_{D_{profile,riblet}}$ = the change in airplane profile drag in percentage (%)
ΔC_f = percent reduction in riblet induced turbulent skin friction (%)
$S_{wet,turb}$= wetted area of airplane covered by turbulent boundary layer (ft^2)
$S_{wet,riblet}$= wetted area of airplane covered by riblets (ft^2)
$\frac{C_{D_{friction}}}{C_{D_{profile}}}$ = ratio of friction drag and profile drag

From this, a probability of percent reduction in riblet induced turbulent skin friction can be determined from the technology characterization detailed in Table 6, which is 5-8% for a wing section and 1-6% for a fuselage [27]. For riblets, this is most likely not a normal distribution due to the variable performance of riblets which are sensitive to off-design conditions, film degradation over time, and/or residue build-up. Thus, for an input parameter distribution, the reduction in profile drag from application of riblets is best reflected as a skewed project evaluation and review techniques (PERT) distribution. A PERT distribution can be defined by the minimum, mode, and maximum values that a variable can take, where in the case of riblets on the wing, a minimum of 2% drag reduction is expected as stated in Ref. [6], a median of 5% and a maximum of 8% from Ref. [27]. These values are substituted into ΔC_f values while $\frac{S_{wet,riblet}}{S_{wet,turb}}$ and $\frac{C_{D_{friction}}}{C_{D_{profile}}}$ vary for each aircraft. Then, with the minimum, mode, and maximum $\Delta C_{D_{profile,riblet}}$ values specified, an input PERT distribution is obtained and input into the MC-GASP framework to obtain the performance distributions.

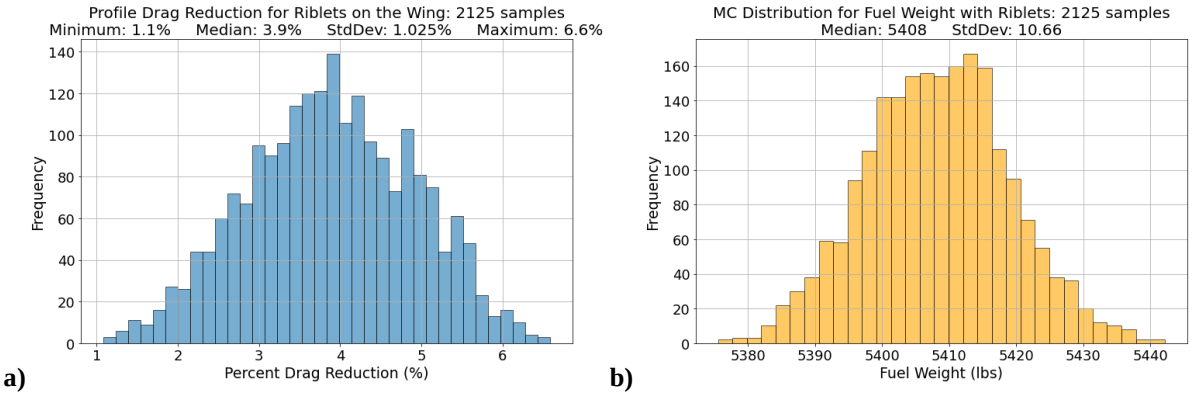

Figure 8. Input and Output PERT Distribution of Riblets Technology Sensitivities on the ATR 42-600

Figure 8a depicts an example of the input probability distribution for riblets in terms of percent drag reduction while Figure 8b depicts the output performance distribution resulting from the coupled MC-GASP performance analysis. The methodology for riblets is repeated for natural laminar flow control, where airfoil profile drag estimation including the effect of laminar flow is modeled based on methods from Torenbeek and Hoerner [35, 36]. The semi-empirical model for minimum profile drag at subsonic conditions is:

$$c_{d,min} = 2C_f[1 + f(t/c)] \quad (4)$$

$$f(t/c) = 2.7\frac{t}{c} + 100\left(\frac{t}{c}\right)^4 \quad (5)$$

Where mean skin friction coefficient C_f can be obtained from Fig. F-4 in Torenbeek or the following chart, which is also programmed in GASP's subroutine for calculating the mean skin friction coefficient as a function of Reynolds number [35]:

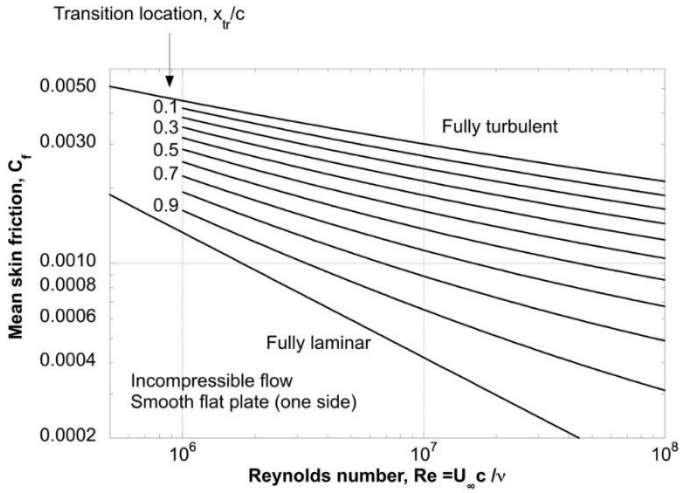

Figure 9. Flat plate skin friction as a function of transition location and chord Reynolds number at incompressible flow conditions

The turbulent flow results are based on the approximate Prandtl-Schlichting equation while the laminar flow results are based on the Blasius equation and the profile drag coefficient is provided as a function of $c_{d,min}$ [37]. The flat plate skin friction is obtained from reading Figure 9.

$$C_f = \frac{0.455}{(\log \mathrm{Re})^{2.58}} - \frac{x_{tr}}{c}\left\{\frac{0.455}{\left[\log\left(\mathrm{Re}\frac{x_{tr}}{c}\right)\right]^{2.58}} - \frac{1.3282}{\sqrt{\mathrm{Re}\frac{x_{tr}}{c}}}\right\} \quad (6)$$

$$c_d = c_{d,min} + k_p(c_l - c_{l,min})^2 \quad (7)$$

Ref. [38] lists typical values for the profile drag to lift parameter k_p which varies significantly with the lift coefficient. However, assuming the application of a cruise flap, the cruise flap will allow the airfoil to operate inside the laminar bucket during cruise and climb. Therefore, $c_d \simeq c_{d,min}$ for Eq. (4).

$$c_d \simeq c_{d,min} = 2C_f\left[1 + 2.7\frac{t}{c} + 100\left(\frac{t}{c}\right)^4\right] \quad (8)$$

To verify the accuracy of the semi-empirical equation for natural laminar flow (NLF), two cases are used for validation

Table 7. Validation for Semi-Empirical NLF Model using NLF(1)-0414F Airfoil

Item	Value
Airfoil Name	NLF(1)-0414F
t/c	0.142
Reynolds Number	10.0 million
Upper/lower surface, x_{tr}	0.70

C_f from Figure 9	0.00113
Semi-Empirical $c_d = c_{d,min}$ from Eq. (8)	0.0032
Experimental Results for $c_{d,min}$ [39]	0.0027

Table 8. Validation for Semi-Empirical NLF Model using HSNLF(1)-0213 Airfoil

Item	Value
Airfoil Name	HSNLF(1)-0213
t/c	0.13
Reynolds Number	9.0 million
Upper/lower surface, x_{tr}	Upper surface x_{tr} = 0.50 Lower surface x_{tr} = 0.70
C_f from Figure 9	0.00141
Semi-Empirical $c_d = c_{d,min}$ from Eq. (8)	0.0039
Experimental Results for $c_{d,min}$ [40]	0.0040

Table 7 and Table 8 show validation for the derived semi-empirical model for NLF using low-speed and high-speed NLF, where for NLF-0414F there is a difference of -0.0005 between the semi-empirical and experimental results, and then a difference of -0.0001 for the HSNLF(1)-0213 results. Overall, fair agreement between semi-empirical method for the prediction of profile drag of laminar flow airfoil and experimental results. Then, the calculation for profile drag reduction with NLF on the fuselage can be determined using similar methodology using Eq.(F-38) of Ref. [35].

$$C_{D_{\text{fuselage}}} = C_f\left(\frac{S_{f_{wet}}}{S_{ref}}\right)(1 + \phi_f) \tag{9}$$

where:

$C_{D_{fuselage}}$ = fuselage profile drag

C_f = skin friction drag coefficient based on x_{tr} using Figure 9 which is x_{tr}=0 for no laminar flow

$S_{f_{wet}}$ = wetted area of the fuselage (ft^2)

S_{ref} = the aircraft reference area (ft^2)

ϕ_f = the fuselage shape factor from Fig. F-9 from Ref. [35] (ft^2)

To determine the impact of NLF on the fuselage as a skewed PERT distribution, calculate the baseline profile drag for each component assuming x_{tr}=0, then x_{tr}=0.50 for the mode, and finally x_{tr}=0.80 as the maximum, as per Table 6. In order to assess aerodynamics technology impacts in GASP, a class of input values referred to as "aerodynamics technology factors" are introduced. Compared to previous methodology, the impacts of aerodynamics technologies were modeled by subtracting from the component wetted area to simulate the effects of skin friction drag reduction. However, drag estimation in GASP has been modified from Ref. [11] to now directly impact the skin friction drag calculation as shown in Eq. (2).

Then, excrescence drag is calculated within GASP where it accounts for 6.59% of the total drag for the ATR 42-600, 6.42% for the Beechcraft 1900D, 6.26% for the DHC-7-100, and 6.56% for the Saab 340B. Within GASP, an aerodynamics technology factor for the excrescence drag, F_{EXCRT}, can be set to the desired percent reduction which is assumed to be a normal distribution. Other technology calibration factors are added for other types of drag in GASP such as interference drag, induced drag, and compressibility drag. Impacts are modeled as distributions due to the potential uncertainty that can be propagated during analytical and experimental data acquisition for aerodynamics technologies, loss of laminar flow from off-design conditions, residue build-up and surface degradation over time, and other factors that may impede the technology's effectiveness.

Since damage-arresting composites (DAC) are a structural technology of interest to the EPFD program, uncertainty quantification of its performance has been done empirically and reported in the technology maturation report (TMR) detailed in Ref. [26]. The purpose of the TMR was to summarize the development and results of recent DAC demonstration to observe the weight savings and fuel burn reduction capabilities of from utilization of lightweight DAC primary structures (wing and fuselage). Though the advanced composites anticipated for this turboprop aircraft

study do not make full use of the PRSEUS technology and omit the use of pultruded rod structures, there are expected weight savings from using stitched composite structures such as DAC that can be modeled using structural technology factors similar to what is done for aerodynamics technology factors. Compared to traditional carbon composites which consist of 20% of the total body weight of the ATR 42-600 and 7% of the body weight of the Saab 340B, DAC is considered an advanced composite with higher weight savings benefits and structural efficiency.

Since the ATR 42-600 and Saab 340B make use of both aluminum and composites for the airframe structure, this must be reflected in the technology factors when modeled semi-empirically. As mentioned in the TMR, sources of uncertainty propagated through the weight estimation environment stem from model fidelity and panel imperfections which lead to variation in material stiffness and densities. Thus, the technology factors provided by the SME, TMR, and Boeing DAC trade study in the ERA report summarized in the TMR capture these bounds which are used in GASP to resize the vehicle [26, 28].

Table 9. Turboprop Aircraft Percent Weight Reduction Distributions from DAC Application

Component	Tech. Factor	Minimum	Mode	Maximum
Wing	Aluminum to DAC ($f_{Al\rightarrow DAC}$)	17%	26%	39%
	Composites to DAC ($f_{C\rightarrow DAC}$)	5%	10%	10.8%
Fuselage	Aluminum to DAC ($f_{Al\rightarrow DAC}$)	6%	16%	30%
	Composites to DAC ($f_{C\rightarrow DAC}$)	7%	10%	10.6%

The composite types used in the construction of each primary structure is detailed above. It is advised that replacement of Kevlar/Nomex structures with DAC will not significantly reduce the structural weight, hence only the sections made of aluminum and carbon-based composites will be replaced with DAC [28]. Table 9 shows the technology factor minimum, mode, and maximum values. The wetted area of sections unaffected by the weight reduction are considered S_{null} for the purpose of the semi-empirical modeling and analysis. Thus, the impact of DAC on the weight of the aircraft is modeled using the semi-empirical equation:

$$W_{\text{struct,DAC}} = W_{struct,baseline}\left[\frac{S_{null}}{S_{struct}} + \frac{S_C}{S_{struct}} f_{C\rightarrow DAC} + \frac{S_{Al}}{S_{struct}} f_{Al\rightarrow DAC}\right] \quad (10a)$$

and

$$S_{null} + S_C + S_{Al} = S_{struct} \quad (10b)$$

where:

$W_{\text{struct,DAC}}$ = weight of the structure (e.g., wing or fuselage) with DAC applied
$W_{\text{struct,baseline}}$ = weight of the structure from GASP given by the detailed breakdown in Table 2
S_{struct} = wetted area of the structure (ft^2)
S_{null} = surface area of the structure where weight reduction from DAC is negligible (e.g., advanced composites already applied or minimum gauge) (ft^2)
S_c = surface area made of composites that can be upgraded to DAC (ft^2)
S_{Al} = area of the structure made of aluminum (ft^2)
$f_{Al\rightarrow DAC}$ = aluminum to DAC technology factor
$f_{C\rightarrow DAC}$ = composites to DAC technology factor

In GASP, the weight trend coefficients for each aircraft component can be modeled as a distribution using Eq. (10) to obtain the sensitivity of DAC on weight reduction and consequent fuel burn reduction on the aircraft. This methodology takes into consideration the wetted area coverage of the structural technology and its areas of impact. Because a key design objective for ERA is to achieve best possible cruise efficiency at minimum cost in structural weight, the impacts of aerodynamic and structural technologies are of utmost importance to model at the preliminary design phase [41]. The next technology, Active Load Alleviation (ALA) is a flight systems technology with both aerodynamic and structural characteristics that aims to reduce maneuver loads (typically a positive design load factor n_{max} = 2.5 g for civil transport jets as in Part 25) and gust loads applied to the airframe.

The stochastic nature of gust loads, estimations in forces and moment calculations, and the ability of the maneuver load control (MLC) system to deploy optimally when encountering in-flight loads are sources of uncertainty propagation in performance assessment of ALA. A semi-empirical model to predict the impact of ALA on aircraft efficiency and weight was determined for the purpose of this study following FAR Part 25 definitions of limit load factors. The weight of an aircraft encountering a vertical gust or executing a turn or pully-up maneuver is given by

$$W = \frac{1}{2}\rho C_L V_c{}^2 Sn \tag{11}$$

where in cruising flight at steady conditions, the load factor is n = 1. Focusing on gust loads, consider a gust speed $\pm U_{de,c}$ at a design cruise speed V_c where according to FAR Part 25, U_{de} = 56.0 ft/s at sea-level, reducing linearly to 44.0 ft/s at 15,000 ft, and reducing linearly to 26.0 ft/s at 50,000ft. As a result of a gust:

$$n = 1 + \frac{\Delta L}{W} = 1 + K_g \frac{C_{L_\alpha} U_{de} 0.5\rho V}{W/S} \tag{12}$$

where:
K_g = the gust alleviation factor
ΔL = change in lift force (lbf)
C_{L_α} = lift curve slope (rad^{-1})
U_{de} = gust speed ft/s
W/S = wing loading (lb/ft^2)

The gust alleviation factor K_g accounts for the fact that the airplane flies into the gust and, hence, the gust does not act on the entire airplane instantaneously.

$$K_g = \frac{0.88\left(\frac{W/S}{C_{L_\alpha} c_{av}\, g\, 0.5\rho_o}\right)}{5.3 + \left(\frac{W/S}{C_{L_\alpha} c_{av}\, g\, 0.5\rho_o}\right)} \tag{13}$$

If U_{de} is specified in ft/s, C_{L_α} in rad^{-1}, the equivalent airspeed V in knots, W/S in lb/ft^2, and ρ = 0.0023769 $slug/ft^3$ FAR Part 25 states that the load factor can be calculated.

$$n = 1 + K_g \frac{C_{L_\alpha} U_{de} V}{498\, W/S} \tag{14}$$

As the load factor n is changed as a result of a maneuver (turn or pull-up) or a gust, the wing root bending moment (WRBM) is changed accordingly. Then, the wing weight can be calculated as a function of the wing-root bending moment, such as demonstrated in Ref. [42], which provided a parametric analysis for studying the effects of wing root bending moment alleviation. Other studies modeling the impact of ALA at the conceptual design phase such as Ref. [12] use multi-point design optimization to determine the optimal design point for an aircraft encountering specific gust and maneuver loads with the goal of minimizing fuel burn. However, a more probabilistic method of accounting for the effects of ALA is favored where in-flight availability of MLC system is considered, which is based on the frequency of exceedance of maneuver load factors per flight determined by NASA from data acquired on three types of jet-propelled civil transports [43]. Within this report, a design load factor of 2.5g without the MLC system activated can be equated with a design load factor of 1.8g for an aircraft with the MLC system on, assuming an in-flight system availability of 99.90%. The maneuver acceleration data from Ref. [43] was plotted with an added curve-fit through the NASA data to obtain the MLC-on versus MLC-off load factor requirements.

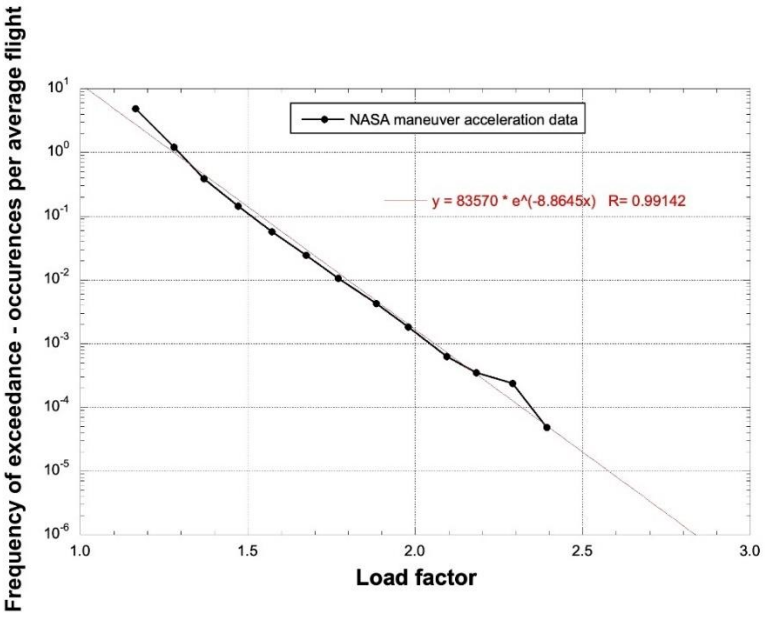

Figure 10. Frequency of maneuver load factor exceedance for civil transport airplanes as determined by NASA based on analysis of in-flight data

Figure 10 depicts the MLC-on versus MLC-off load factor requirements for a range of system availabilities with the earlier equivalence (2.5g to 1.8g) highlighted in red. As a second example, if a load factor combination of $n_{MLC\text{-}on}$ =2.535 and $n_{MLC\text{-}off}$ =1.350 is selected, an availability of 99.9990% would be required. Thus, to simulate the effects of an ALA system, a PERT distribution is used where for the best-case scenario, a design load factor of 2.5g without the MLC system activated can be equated with a design load factor of 1.8g which is a 28% decrease in GASP model's load alleviation factor with a mode of 20% (2.0g).

Lastly, the capability of modeling performance distributions from application of advanced propulsion technologies was demonstrated. The advanced turboprop engines are based on scalable turboprop engine models developed in NPSS for Ref. [7], which is based on published technology projections that assume evolutionary improvements in engine cycle and materials that lead to overall lower fuel burn and specific engine dry weight [34]. The advanced turboprop engine models in NPSS assumed fixed engine architecture, improved OPR and turbine temperatures, improved component efficiencies (e.g., compressor and turbine), turbine cooling technologies, and engine weight projections from Refs. [34, 44]. With these combined improvements, a 15% improvement in brake-specific fuel consumption (BSFC) could be assumed [8]. However, without the use of NPSS and to account for uncertainty in these estimations, the expected engine performance was set at a mode of 10% improvement in BSFC with a maximum of 15% BSFC while the specific engine weight was expected to vary from 2-4% to account for the lower and upper bounds of the technology projections estimates. In GASP, this is done by impacting the form factor for installed engine fuel flow and the maximum sea level static horsepower parameters [11].

B. Monte Carlo-GASP Simulation Framework

With the baseline turboprop configurations parametrically synthesized in GASP, mission profiles established, and advanced aircraft technology models finalized, performance assessment of advanced turboprop configurations infused with advanced technologies was conducted. Within Python, a MC interface was developed around GASP to set up the MC-GASP simulation framework able to take input parameter distributions, run calculations in GASP to obtain aircraft performance metrics, and output performance distributions with uncertainty.

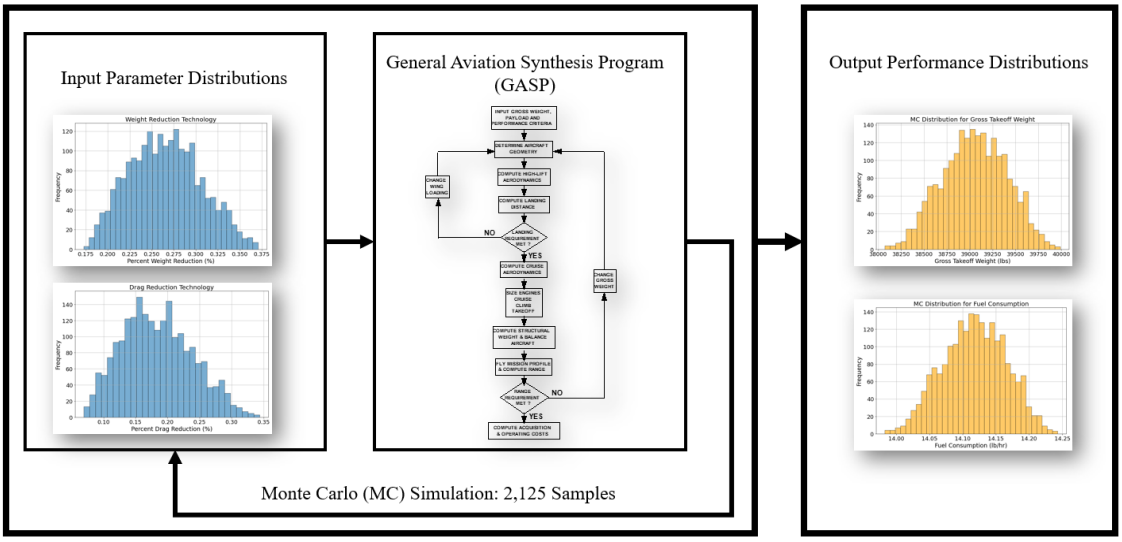

Figure 11. Monte Carlo-GASP Simulation Framework

Figure 11 shows the Monte Carlo-GASP simulation workflow. Technology sensitivity studies were conducted for each turboprop configuration in Table 1 of each independent technology in Table 5. Aggregate technology build-ups were also performed to demonstrate the capability of analyzing multiple technologies simultaneously and analyzing cumulative impact on aircraft performance.

V. Results and Discussion

The individual and aggregate performance benefits of each technology on gross takeoff weight (GTOW), operating empty weight (OEW), and fuel weight are shown for each turboprop configuration. Since the output of the MC-GASP simulations are performance distributions with uncertainty, box and whisker plots are used to capture the distribution of data, where the whiskers capture the range of values, the center line of the box depicts the 50th percentile (median), and the edges of the box show the first quartile and third quartiles respectively. For this study, 2,125 samples were sufficient in characterizing the input and output distributions.

A. Gross Takeoff Weight Technology Sensitivity Studies

For the 19 passenger Beechcraft 1900D, the aggregate technology weight takeoff for GTOW ranged from 9.83% to 16.8% with a median of 13.5%, with the highest contributions stemming from DAC (3.57% to 11.5% with a median of 7.15%.) From Ref. [7], riblets were expected to have a 0.4% reduction on the overall GTOW for the B1900D, which falls within the third quartile of results from the MC-GASP analysis. Figure 12 shows the results for the GTOW sensitivity studies for all four turboprop configurations.

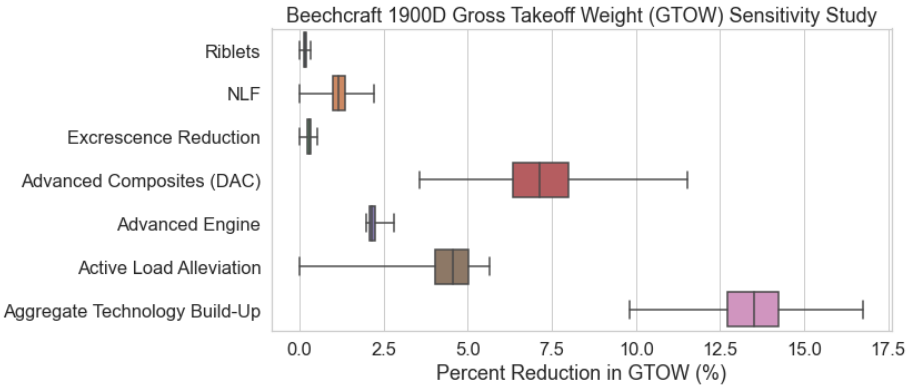

a) Beechcraft 1900D

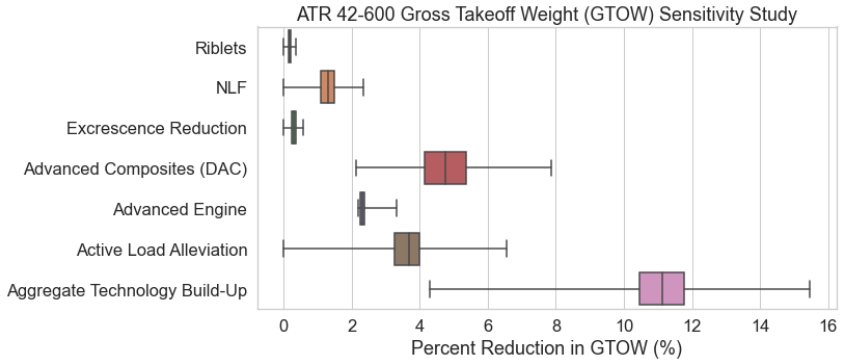

b) ATR 42-600

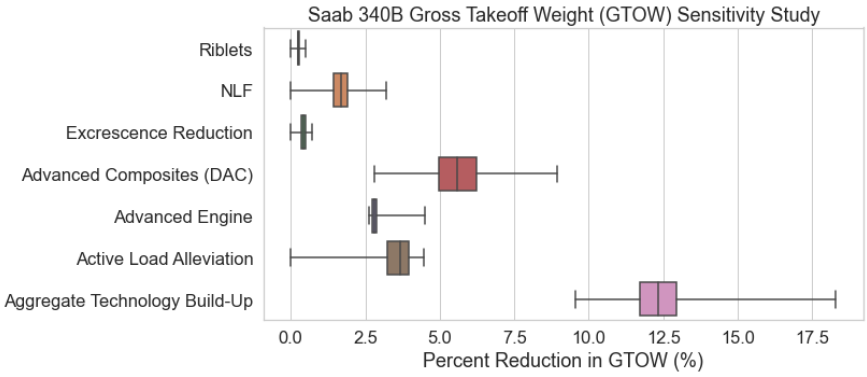

c) Saab 340B

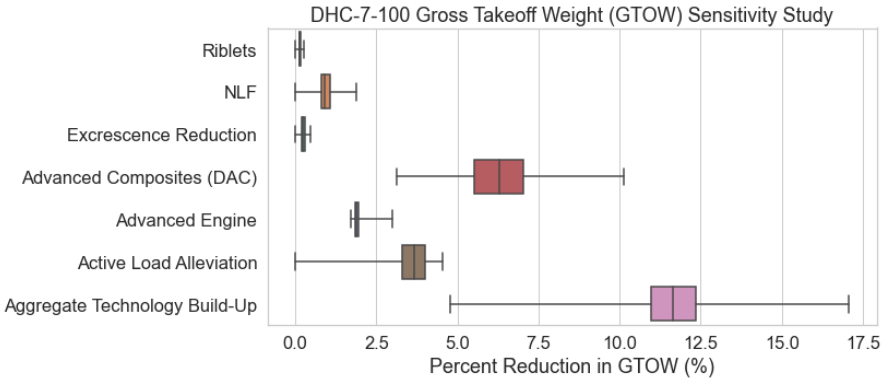

d) DHC-7-100

Figure 12. Gross Takeoff Weight Technology Sensitivity Studies

For the aggregate technology benefit on GTOW for the ATR 42-600, the minimum was 4.28% to a maximum of 15.46% reduction with a median of 11.10%, showing that the median fell closer to the maximum than the minimum. In Ref. [7], NLF was predicted to have a 1.8% GTOW reduction on the ATR 42-600 whereas in this study, NLF had a minimum of 0% GTOW reduction, maximum of 2.33% reduction, with a median of 1.3%, showing that the value of 1.8% fell between the third quartile and maximum. For the Saab 340B, the aggregate technology benefit ranges from 9.54% to 18.3% GTOW reduction with a median of 12.3% with a first and third quartile GTOW reduction of 11.7% and 12.9% respectively. Lastly, for the DHC-7-100, the aggregate technology benefit ranges from 4.76% to 17.1% GTOW reduction with a median of 11.6%. The 25th percentile GTOW reduction for the DHC-7-100 is 11% while the 75th percentile GTOW reduction is 12.3%.

Overall, the technology sensitivity studies show that the most effective technology for reduction in GTOW is advanced composites (DAC) followed by ALA. This is expected as structural weight accounts for most of the GTOW and technologies that impact structural weight of primary components such as DAC and ALA will have the highest impact. The aggregate technology build-up depicts the propagation of uncertainties when analyzing the individual technologies in a package. The benefit of the box-and-whisker plot visualization of the results allows for improved conceptualization of not only the performance benefit, but also the width of the range of expected performance and where the median performance benefit falls in the distribution. For instance, the expected benefits for the advanced engine ranges between 1.96% GTOW reduction and 2.79% reduction, but the median fall closer to the minimum at 2.15% GTOW reduction. When assessing the benefits of an in-development technology at the conceptual design phase, this methodology rationally presents a way to inform decision-makers of not only the technology's impact but uncertainty present in preliminary results.

B. Operating Empty Weight (OEW) Technology Sensitivity Studies

The operating empty weight is the weight of an aircraft when empty of fuel and payload. Similarly, to gross takeoff weight, it is an important top-level parameter that dictates fuel efficiency, payload capacity, maintenance costs, and must fall within weight limits with regards to regulatory compliance.

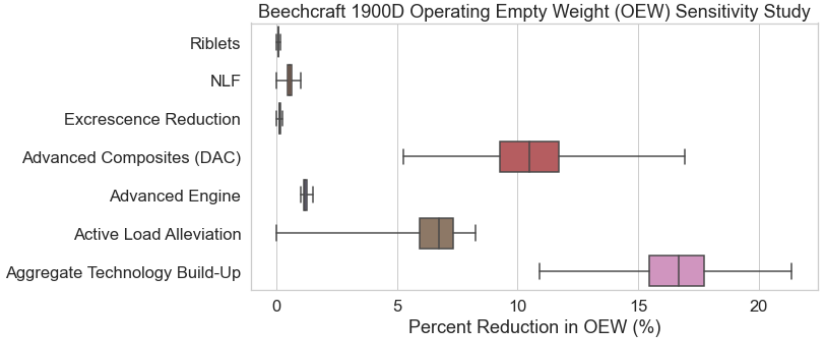

a) Beechcraft 1900D

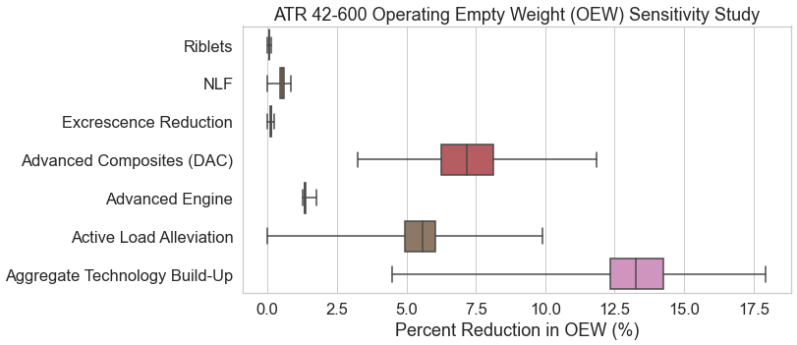

b) ATR 42-600

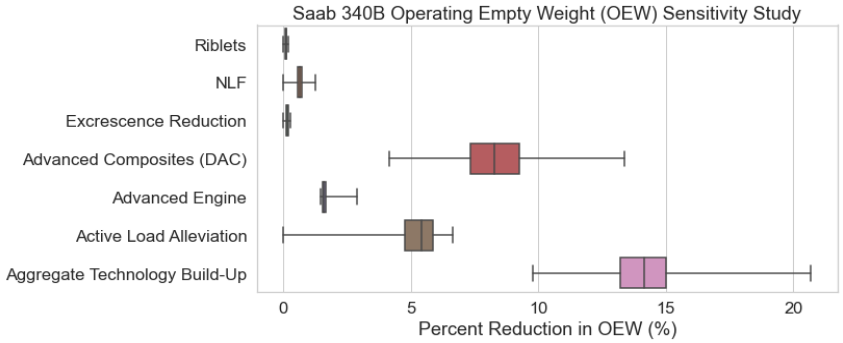

c) Saab 340B

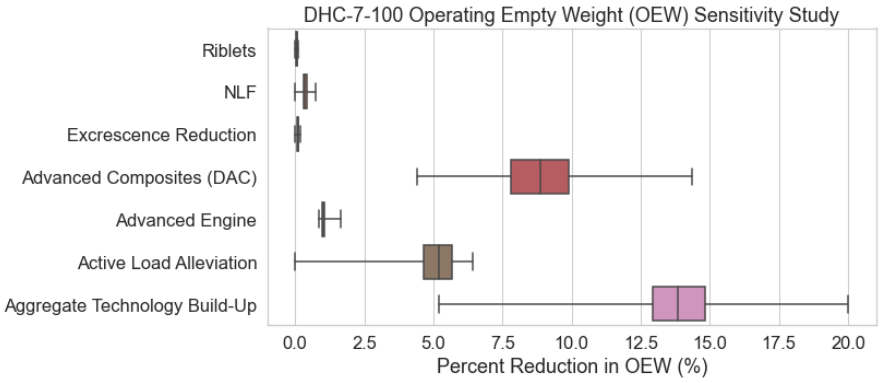

d) DHC-7-100

Figure 13. Operating Empty Weight Technology Sensitivity Studies

For Figure 13a, the aggregate technology benefit for the Beechcraft 1900D ranges from 10.9% to 21.4% with a median of 16.7% OEW reduction, with the greatest contribution from DAC and ALA. For the larger turboprop aircraft, the DHC-7-100 aggregate technology benefit for OEW varies between a minimum of 5.21% to a maximum of 20% OEW reduction with a median of 13.9%. This is similar to the ATR 42-600, a similarly sized aircraft which ranges from a 4.5% to 18% OEW reduction with a median of 13.3%. These results are expected as the B1900D's airframe consists of conventional metal structures, while the ATR 42-600 for instance, has a 20% composite body weight [45]. Then, for the Saab 340B which as a 7% composite body weight, the aggregate OEW reduction ranges from 9.8% to 20.7% with a median of 14.1% reduction. With less of its body weight in composites, the weight savings from DAC are higher compared to that of the ATR 42-600. This is captured in the semi-empirical models used in this study.

C. Fuel Weight Technology Sensitivity Studies

The definition of fuel weight in this study represents the total fuel load which includes both the primary mission and reserves. Essentially, it is the fuel used up to the end of the final descent. From this total fuel weight, the ICAO methodology for estimating of the amount of CO_2 emissions from a flight can be used, which is dictated by the following equation [46].

$$CO_2\ per\ pax = \frac{3.16\left(W_{Fuel_{total}} * f_{pax-to-freight}\right)}{f_{pax_{load}} * n_{seats}} \quad (15)$$

where:
$W_{Fuel_{total}}$ = total fuel (lbf)
$CO_2\ per\ pax$ = CO_2 emissions (tonnes)
$f_{pax-to-freight}$ = ratio calculated from ICAO statistical database based on the number of passengers and the tonnage of mail and freight
$f_{pax_{load}}$ = the ratio calculated from ICAO statistical database based on number of passengers transported and the number of seats

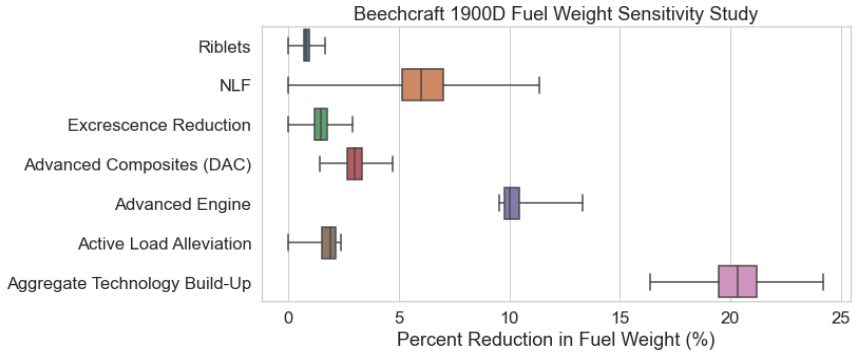

a) Beechcraft 1900D

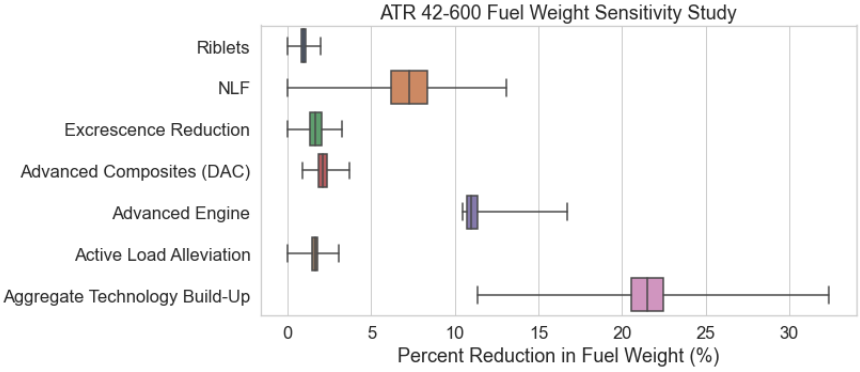

b) ATR 42-600

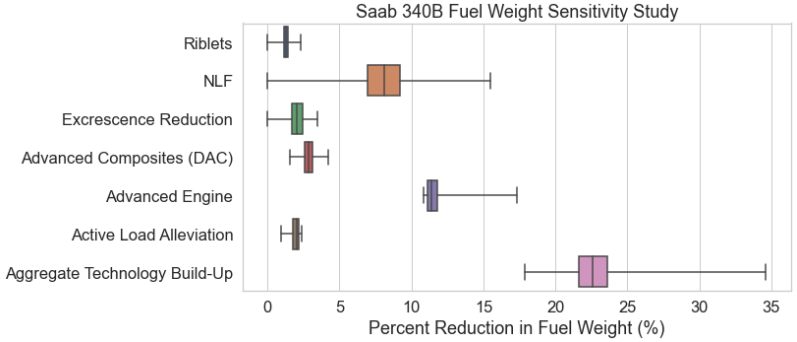

c) Saab 340B

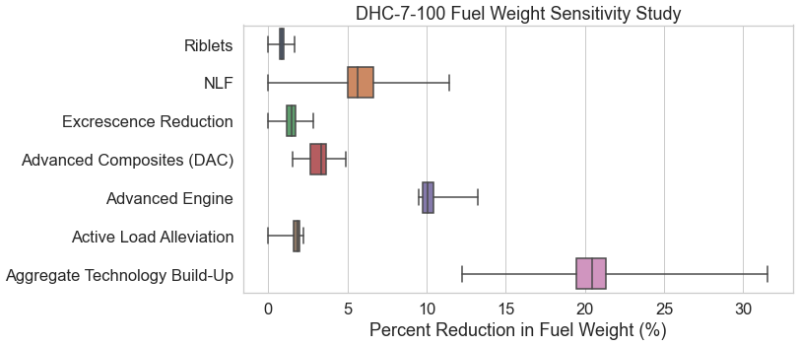

d) DHC-7-100

Figure 14. Fuel Weight Technology Sensitivity Studies

For Eq. (15), 3.16 is a constant representing the number of tonnes of CO_2 produced by burning a tonne of aviation fuel. For the total fuel weight sensitivity in Figure 14, the highest impact technology is the advanced turboprop engine as it directly impacts fuel burn metrics. Percent reduction in fuel weight is proportional to CO_2 emissions as defined by Eq. (15).

Table 10. Percent Fuel Weight Reduction for Technology Sensitivity Studies

Advanced Technology	Percent Fuel Reduction: Minimum % to Maximum % (Median %)			
	Beechcraft 1900D	**ATR-42-600**	**Saab 340B**	**DHC-7-100**
Riblets	0% to 1.68% (0.82%)	0% to 2% (0.97%)	0% to 2.33% (1.25%)	0% to 1.65% (0.85%)
NLF	0% to 11.4% (6.02%)	0% to 13.1% (7.25%)	0% to 15.5% (8.13%)	0% to 11.5% (5.62%)
Excrescence Reduction	0% to 2.89% (1.46%)	0% to 3.25% (1.67%)	0% to 3.48% (2.05%)	0% to 2.83% (1.48%)
Advanced Composites	1.43% to 4.70% (3%)	0.90% to 3.68% (2.11%)	1.59% to 4.23% (2.85%)	1.56% to 4.91% (3.32%)
Advanced Engine	9.5% to 13.3% (10.0%)	10.5% to 16.7% (11%)	10.9% to 17.3% (11.38%)	9.5% to 13.2% (10.04%)
Active Load Alleviation	0% to 2.39% (1.91%)	0% to 3.06% (1.65%)	0% to 2.39% (2.02%)	0% to 2.27% (1.84%)
Aggregate Technology Build-Up	16.4% to 24.2% (20.3%)	11.4% to 32.4% (21.5%)	17.9% to 34.6% (22.6%)	12.3% to 31.6% (20.4%)

The aggregate technology impacts range from a 50^{th} percentile fuel weight reduction of 20.3% to 22.6%, where significant contribution to fuel burn reduction stemmed from the advanced engine cycle and materials and natural laminar flow control. It is worth mentioning that depending on anti/de-icing mechanism used for the baseline aircraft (i.e. pneumatic boot-based de-icing systems) NLF may be incompatible. Then, using Eq. (15) and assuming Intra-North American routes from Ref. [46], the percent reduction in CO_2 emissions can be calculated for the aggregate technology benefit.

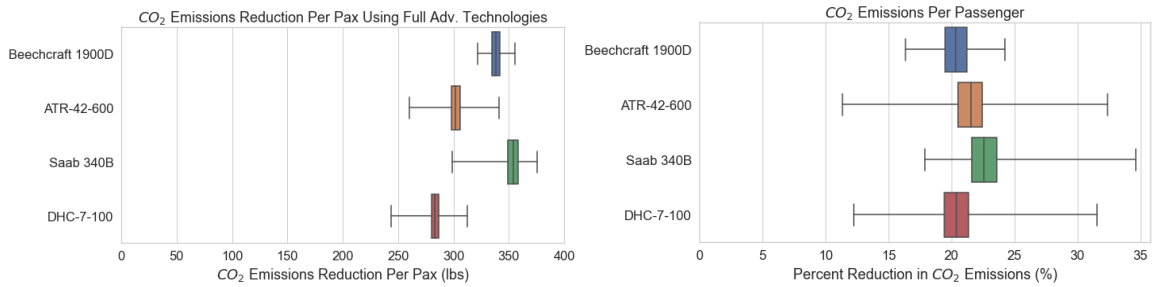

Figure 15. Aggregate Percent Reduction in Carbon Dioxide Emissions Per Passenger for Advanced Turboprops

In Figure 15, the aggregate technology benefits appear to increase for configurations with higher design capacity with percent reduction in CO_2 emissions having the same magnitude as the values reported in Table 10. The aggregate technology build-up was used for the advanced vehicle model and compared to the baseline vehicle model to observe the overall estimated performance impacts.

Table 11. Advanced Vehicle 50th Percentile Performance Parameters from GASP

Performance Parameter (% Diff.)	Beechcraft 1900D	ATR 42-600	DHC-7-100	Saab 340B
AEO T.O. distance, ft	1947 (-13.5%)	2895 (-8.47%)	1475 (-30.1%)	2352 (-24.1%)
CEI T.O. distance, ft	2029 (-14.5%)	3228 (-11.1%)	1507 (-31.7%)	2705 (-15.7%)
Accelerate-Stop distance, ft	2550 (-5.55%)	3428 (-5.67%)	2369 (-10.4%)	2780 (-6.93%)
2nd Segment CEI Rate -of-climb, fpm	786 (-0.63%)	459 (+16.5%)	1008 (-0.4%)	545 (+62.9%)
Time to Climb to Cruise Altitude, min	11.11 (-28%)	13.47 (32.7%)	12.66 (-32.8%)	12.09 (-6.13%)
Cruise Speed, ktas	250 (0%)	200 (0%)	220.5 (0%)	252 (0%)
Cruise Lift-to-Drag Ratio	16.49 (+9.42%)	19.84 (+38%)	20.75 (+32.2%)	16.82 (+16.1%)
Equivalent Flat Plate Area, ft^2	6.3120 (-24.5%)	9.2123 (-39%)	12.28 (-41.6%)	9.890 (-18.8%)
Breguet Range Factor, nm	9174 (+24.36%)	13,794 (+49.6%)	11,839 (41.3%)	11,224 (+25.7%)
Specific range, nm/lb	0.6086 (+38.6%)	0.34093 (+48.6%)	0.2977 (+53.8%)	0.39157 (+25%)
BSFC, lb/hr/hp	0.5619 (-7.14%)	0.4156 (-11%)	0.5057 (-11.8%)	0.4508 (-7.11%)
TSFC, lb/hr/lbf	0.4701 (-7.91%)	0.4298 (-7.69%)	0.3867 (-6.48%)	0.3779 (-7.01%)

Compared to Table 4, significant reductions in T.O distances, cruise L/D, and propulsive efficiency in TSFC and BSFC are observed for the advanced configurations. For configurations with higher design capacities, the performance benefits appear to increase. It is assumed in these analyses, the payload is kept constant between the baseline and advanced turboprop configurations.

VI. Conclusion

Parametric baseline models of four selected turboprop configurations (Beechcraft 1900D, ATR 42-600, DHC-7-100, and Saab 340B) were established in a physics-based M&S environment and calibrated against publicly available data. Capabilities of the NASA-developed vehicle synthesis and mission analysis code GASP was demonstrated, with baseline performance levels established and validated by comparison of GASP results with published flight envelopes. Advanced aircraft technologies were identified and modeled within GASP using semi-empirical modeling and Monte-Carlo simulation to account for uncertainty propagation. The semi-empirical models used to project technology characterization metrics onto the 3D aircraft components was detailed for aerodynamics, structures, flight systems, and propulsion technologies.

For this study, 2,125 MC cases were used to estimate the performance distribution for each technology. The impacts of advanced aircraft technologies on top-level aircraft specifications such as gross weight, empty weight, and fuel weight were presented, which can be used to obtain expected performance estimates for CO_2 emissions reduction. For the aggregate technology portfolio used in this study, potential CO_2 emissions reductions ranged from ~15-20% reduction for the 19 pax configuration and ~18%-35% for the 34 pax configuration, and ~10-35% for the 48-50 pax

configurations. Additionally, significant fuel burn savings from application of aerodynamics and propulsion technologies was observed. The capabilities of capturing performance uncertainties, modeling advanced technologies and turboprop models in systems analysis were detailed and documented. The results of this work will serve as benchmark cases in the robust assessment of EAP technology performance impacts with uncertainty quantification for electrified or hybridized aircraft configurations.

References

[1] Federal Aviation Administration (FAA), "The United States Climate Action Plan," 9 November 2021. [Online]. Available: https://www.faa.gov/sites/faa.gov/files/2021-11/Aviation_Climate_Action_Plan.pdf.

[2] NASA Aeronautics Research Mission Directorate (ARMD), "Strategic Implementation Plan," 2019.

[3] NASA Aeronautics Mission Directorate (ARMD), "Electrified Powertrain Flight Demonstration," 19 April 2022. [Online]. Available: https://www.nasa.gov/aeroresearch/programs/iasp/epfd.

[4] U.S. Department of Transportation, "Essential Air Service," 22 November 2017. [Online]. Available: https://www.transportation.gov/policy/aviation-policy/small-community-rural-air-service/essential-air-service.

[5] NASA Aeronautics Research Mission Directorate, "Advanced Air Transport Technology (AATT) Project," 6 August 2017. [Online]. Available: https://www.nasa.gov/aeroresearch/programs/aavp/aatt/description/.

[6] Mavris, D. et al., " FY2019 Advanced Air Transportation Technologies Systems Analysis Report: Technology Portfolio," Georgia Tech Aerospace Systems Design Laboratory, 2019.

[7] Cai, Y., Xie, J., and Mavris, D., "Advanced 2030 Turboprop Aircraft Modeling for the Electrified Powertrain Flight Demonstration program," in *AIAA SCITECH 2022 Forum*, Anaheim, CA, 2022.

[8] *Personal communication with Y. Cai and J. Gladin, Georgia Tech ASDL*. [Interview]. March 2022.

[9] Green, Lawrence L., Lin, Hong-Zong, and Khalessi, Mohammad R., "Probabilistic Methods for Uncertainty Propagation Applied to Aircraft Design," NASA NTRS, Hampton, VA, 2003.

[10] Lenz, Annelise and Crossley, William, "Simple Uncertainty Propagation for Early Design Phase Aircraft Sizing," in *9th AIAA Technology, Integration, and Operations Conference (ATIO)*, Hilton Head, SC, 2009.

[11] Hague, D., "GASP – General Aviation Synthesis Program. Volume 1: Main Program. Part 1: Theoretical Development," Technical Report NASA-CR-152303-VOL-1-PT-1, National Aeronautics and Space Administration, 1978.

[12] Xu, Jia and Kroo, Ilan, "Aircraft Design with Active Load Alleviation and Natural Laminar Flow," in *53rd AIAA/ASME/ASCE/AHS/ASC Structures, Structural Dynamics and Materials Conference*, Honolulu, HI, 2012.

[13] NASA, "Monte Carlo Simulation," Katherine Johnson IV&V Facility, 23 August 2017. [Online]. Available: https://www.nasa.gov/centers/ivv/jstar/monte_carlo.html. [Accessed 27 March 2023].

[14] magniX, "magniX Announces Milestone in NASA Program to Accelerate Electric Flight Technologies for Commercial Aviation," PR Newswire, 28 April 2022. [Online]. Available: https://www.prnewswire.com/news-releases/magnix-announces-milestone-in-nasa-program-to-accelerate-electric-flight-technologies-for-commercial-aviation-301535812.html. [Accessed 29 March 2023].

[15] Norris, Guy, "GE Partners With Boeing, Aurora For Electric Power Flight Demo," Aviation Week, 22 April 2022. [Online]. Available: https://aviationweek.com/aerospace/emerging-technologies/ge-partners-boeing-aurora-electric-power-flight-demo. [Accessed 29 March 2023].

[16] Taylor, J. W. R., Jane's All The World's Aircraft 1982–83 (ISBN 0-7106-0748-2), London: Jane's Yearbooks , 1982.

[17] Raytheon, "Specifications and Performance Beechcraft 1900D Passenger," Raytheon, Arlington County, VA, 2012.

[18] ATR, "ATR 42-600," ATR, 12 April 2020. [Online]. Available: https://www.atr-aircraft.com/wp-content/uploads/2020/07/. [Accessed 28 March 2023].

[19] XdH Aviation Services Inc. , "de Havilland DHC-7 Dash-7," XdH Aviation Services Inc. , 8 September 2002. [Online]. Available: http://www.xdh.ca/DHC_Aircraft/DHC-7/dhc-7.html. [Accessed 15 January 2018].

[20] SAAB Technologies, "SAAB 340B/Bplus," Saab Aircraft Leasing, 23 April 2009. [Online]. Available: https://www.saabaircraftleasing.com/prod/datasheets/340b_jar.pdf. [Accessed 21 May 2022].

[21] Thomas, George, "NPSS Power System Library Overview," NASA Glenn Research Center, Power Management and Distribution Branch (LEM), Cleveland, OH, 2020.

[22] Worobel, R., "Hamilton Standard Prop Code: Computer Program User's Manual for Advanced General Aviation Porpeller Study," NASA CR-2066, 1972.

[23] Pratt & Whitney , "P&W Canada PT6A EASA Type-Certificate Data Sheet, Issue 6," EASA.IM.E.008, 2022.

[24] IATA, "Aircraft Technology Roadmap to 2050," International Air Transport Association, Geneva, Switzerland, 2019.

[25] ICAO, "INDEPENDENT EXPERT INTEGRATED TECHNOLOGY GOALS ASSESSMENT AND REVIEW FOR ENGINES AND AIRCRAFT," International Civil Aviation Organization, Montreal, CA, 2019.

[26] Jegley, Dawn C. and Corman, Jason A., "Technology Maturation Report for Damage Arresting Composites under the Environmentally Responsible Aviation Project," NASA/TM–20220015363, Hampton, VA, 2022.

[27] Viswanath, P., "Aircraft Viscous Drag Reduction Using Riblets," Progress in Aerospace Sciences, 38(6/7), 571-600, 2002.

[28] D. Jegley, Interviewee, *Personal communication with D. Jegley, NASA Langley Advance Structures Branch, Feb, 2021.*. [Interview]. 2021.

[29] Georgia Tech ASDL Midterm Report, "Systems Analysis Support for the Electrified Powertrain Flight Demonstrator Program," 2021.

[30] van Zante, D. and Collier, F., "The Environmentally Responsible Aviation (ERA) Project - A Technology Development Project," Technical Report GRC-E-DAA-TN35219, 2017.

[31] Kerho, Michael and Kramer, Brian, "Enhanced Airfoil Design Incorporating Enhanced Airfoil Design Incorporating Boundary Layer Mixing Devices," in *41st Aerospace Sciences Meeting and Exhibit*, Reno, NV, 2003.

[32] Coder, James G. and Somers, Dan M., "Design of a slotted, natural-laminar-flow airfoil for commercial transport applications," *Aerospace Science and Technology*, vol. 106, no. 20, pp. 1-11, 2020.

[33] Goldhammer, M.I., and Plendl, B.R, "Boeing, Surface Coatings and Drag Reduction," *Aero Magazine*, pp. 15-20, 49 Quarter 1 2021.

[34] Welch, Gerard E. et al., "Rotary-Wing Relevant Compressor Aero Research and Technology Development Activities at Glenn Research Center," NASA/TM—2012-217280, Cleveland, OH, 2012.

[35] Torenbeek, E., Synthesis of Subsonic Airplane Design, Delft University of Technology: Springer, 1982.

[36] Hoerner, S. F., Fluid-Dynamic Drag, Bakersfield, CA: Hoerner Fluid Dynamics, 1965.

[37] Schlichting, H., Boundary Layer Theory, 7th Edition, McGraw-Hill, 1979.

[38] Yates, J.E., and Donaldson, C., "A Fundamental Study of Drag and an Assessment of Conventional Drag due to Lift Reduction Devices," NASA CR-4004, 1986.

[39] McGhee, R.J, Viken, J.K, Pfenninger, W., Beasley, W.D., and Harvey, W.D, "xperimental Results for a Flapped Natural Laminar Airfoil with High Lift to Drag Ratio," NASA-TM-85788, 1984.

[40] Sewall, W.G., McGhee, R.J., Viken, J.K., Waggoner, E.G., Walker, B.S., and Millard, B.F., "Wind Tunnel Results for a High-Speed, Natural Laminar-Flow Airfoil Designed for General Aviation Aircraft," NASA-TM-87602, 1985.

[41] Collier, F., "Environmentally Responsible Aviation for Environmental Challenges Facing Aviation," in *Report NF1676L-1123, GARDN, First Green Aviation Conference*, 2011.

[42] Heyson, H.H, Riebe, G.D., and Fulton, C.L, "Theoretical Parametric Study of the Relative Advantages of Winglets and Wing-Tip Extensions," NASA TP-1020, 1977.

[43] Ramsey, H.D., and Lewolt, J.G, "Design Maneuver Loads for an Airplane with an Active Control System," AIAA Paper 79-0738, 1979.

[44] Clarke, David R. et al., "Thermal-barrier coatings for more efficient gas-turbine engines," *MRS Bulletin,* vol. 37, pp. 891-898, 2012.

[45] Castanie, Bruno, Bouvet, Christophe, and Ginot, Malo, "Review of Composite Sandwich Structure in Aeronautic Applications," Composites Part C: Open Access, 2020.

[46] ICAO, "ICAO Carbon Emissions Calculator Methodology Version 11," International Civil Aviation Organization, Montreal, CA, 2018.

[47] Nordin, Pontus, "Saab experience with application of composites in aerospace structures," ICAS Biennial workshop 2011, Stockholm, Sweden, 2011.